Optical gain in monodispersed silicon nanocrystals

M. Cazzanelli,[a] D. Navarro-Urriós, F. Riboli, N. Daldosso, and L. Pavesi
INFM-Dipartimento di Fisica, Università di Trento, via Sommarive 14, I-38050 Povo (Trento), Italy

J. Heitmann, L. X. Yi, R. Scholz, M. Zacharias, and U. Gösele
Institute of Microstructure Physics, Max Planck Institute, Weinberg 2, 06120 Halle, Germany

(Received 22 January 2004; accepted 15 June 2004)

Stimulated emission from silicon-nanocrystal planar waveguides grown via phase separation and thermal crystallization of SiO/SiO_2 superlattices is presented. Under high power pulsed excitation, positive optical gain can be observed once a good optical confinement in the waveguide is achieved and the silicon nanocrystals have proper size. A critical tradeoff between Auger nonradiative recombination processes and stimulated emission is observed. The measured large gain values are explained by the small size dispersion in these silicon nanocrystals. © *2004 American Institute of Physics*. [DOI: 10.1063/1.1781770]

I. INTRODUCTION

The evolution of microelectronic circuits is currently limited by several factors. One of these is the interconnect bottleneck due to the inability to transfer data at increasing speed in microelectronic circuits. One possible solution for this problem is the substitution of metallic wires with optical channels.[1,2] Today, this is possible only within a hybrid approach where compound semiconductor based emitters are integrated within the silicon microelectronic chip. It would be very interesting to replace compound semiconductors with silicon based light emitters or, possibly, lasers.[2] Given the recent demonstration of stimulated emission in silicon nanocrystals (Si-nc),[3–7] Si-nc represent a possible approach to have a silicon laser operating at around 750 nm[2]. The experimental work in this field has developed very rapidly.[3–10] Some aspects related to this unexpected stimulated emission have been criticized.[11,12] A scientific debate is also focusing on the understanding of its physics.[2] The lowering of the dimensionality of crystalline silicon in Si-nc, together with their interaction with the embedding matrix (usually SiO_2), has been invoked to explain the high emission efficiency and the observation of net optical gain. The optical gain has been tentatively attributed to localized radiative states formed by oxygen-silicon bonds at the Si-nc surface within a four level recombination model.[4,13,14]

We present an experimental effort to look for optical gain in a particular class of silicon nanocrystals produced by a method which guarantees a small size dispersion. The technique is based on the crystallization of amorphous SiO/SiO_2 superlattices and results in high luminescent Si-nc with an atypically low size dispersion.[15]

II. SAMPLES

A set of six superlattice samples grown using the recently developed technique of evaporation followed by phase separation and crystallization of silicon nanocrystals, driven by high temperature annealing, has been prepared. Table I reports their main growth parameters. All have an active superlattice layer where the Si-nc are formed. The superlattice is formed by repeated depositions of nanometer thick amorphous silicon mono-oxide or silicon dioxide layers. They were formed by deposition either on a quartz substrate (A–D) or on a silicon wafer (E and F), in a conventional evaporation system with two symmetrically arranged evaporators. Rotation of the substrate enables a high homogeneity (better than 10%) over the whole 4 in wafer. Before evaporation, the chamber was pumped down 1×10^{-7} mbar. The substrate temperature during deposition was 100 °C. More details on the growth method and apparatus are reported in Ref. 15. The thicknesses of the various layers in the sample and other nominal growth parameters are shown in Table I (upper rows). In samples A–D, the active superlattice layer is deposited on a thick SiO_2 layer, while in samples E and F the active layer is embedded between two thick layers of deposited SiO_2. After deposition, the samples were annealed at 1100 °C for 1 h in N_2 atmosphere to induce phase separation and Si crystallization in the superlattice layers.[16] The peculiarity of this method is the high control on the size of the Si-nc, which show a small size dispersion.

An example of a transmission electron microscopy (TEM) image for sample F is shown in Fig. 1. In the superlattice layer, Si nanocrystals are observed to have sizes determined by the deposited amorphous SiO layer thickness. During the annealing, some oxidation takes place at the interface between the deposited layer and the quartz or air. For this reason, the final sample structure slightly differs from the nominal one. TEM analysis allows a careful determination of the thickness of the various layers in the samples (Table I, bottom rows).

We measured the transmittance (T) and the reflectance (R) in a wide spectral range for those samples grown on a transparent substrate. The results are reported in Fig. 2. Interference fringes are observed up to 300 nm. Using these experimental data and neglecting light diffusion, the absorbance $A=100-T-R$ can be estimated (see inset in Fig. 2). As the size of the Si-nc increases (see Table I and nominal

[a]Electronic mail: kazza@science.unitn.it;
URL; http://www/science.unitn.it/~semicon/

TABLE I. Nominal growth parameters and parameters extracted from cross sectional TEM for the studied samples. d_{SiO} is the nominal thickness of the amorphous silicon mono-oxide deposited layers, d_{SiO_2} is the nominal thickness of the silica layers, N_{SiO} and N_{SiO_2} are the number of SiO and SiO_2 layers in the active superlattice.

	Nominal growth parameters					
Sample name	A	B	C	D	E	F
	2	3	4	5	2	4
d_{SiO_2} (nm)	5	5	5	5	2	4
N_{SiO}/N_{SiO_2}	45/46	45/46	45/46	45/46	42/43	30/31
Substrate	Quartz	Quartz	Quartz	Quartz	Silicon	Silicon
	TEM data					
Bottom oxide thickness (nm)	25	25	71	11	79	310
Superlattice thickness (nm)	152	186	214.5	295	177	213
Top oxide thickness (nm)	69.5	68	14	25.5	71	195
Total measured thickness (nm)	247	270	291	331	327	690

parameters), the absorbance edge shifts to lower energies in accordance to a simple quantum confinement model of the electronic properties of Si-nc.

III. WAVEGUIDE CHARACTERIZATION

As the samples were grown in a waveguide structure, we characterized their waveguiding properties with a prism-coupling (*m*-line) technique at 632.8 nm.[17] The optical parameters are then extracted with a simulation software and a model of the optical anistropy for the multilayer structure.[18,19]

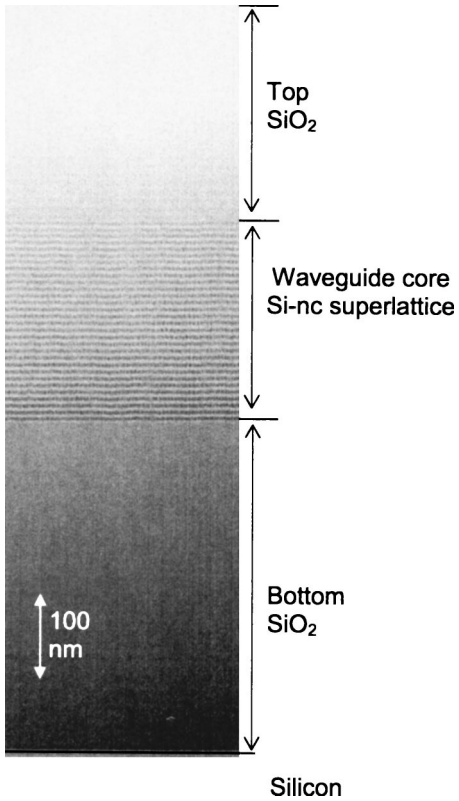

FIG. 1. Transmission electron microscopy (TEM) cross section photograph of sample F.

m-line measurements allow measurement of the effective refractive index for the optical guided moded. No guided modes were observed in samples E, F, and A, while samples B, C, and D showed only one mode with the two polarizations (TE and TM). The associated effective refractive indices n_{TE} and n_{TM} are reported in Table II and Fig. 3(a). The modal birefrigence, defined as $B=n_{TE}-n_{TM}$ can be also extracted. As one can see both the effective refractive indices and the modal birefringence increase as the Si-nc size increases.

Using the Si-nc data extracted from the TEM images and the nominal growth parameters, we reproduced the observed effective refractive indices by using a waveguide simulator and assuming an optical birefringent waveguide core. The waveguide core is formed by the Si-nc superlattice, which is inherently birefringent (form birefringence) due to its layered structure (Fig. 1).[20] The Si-nc superlattice behaves like a uniaxial crystal (with its optic axis along the deposition direction) with ordinary n_o and extraordinary n_e refractive indices. A summary of the extracted theoretical data is shown in Table II. As expected from the nominal parameters (Si content and thickness),[21] sample D has the highest filling

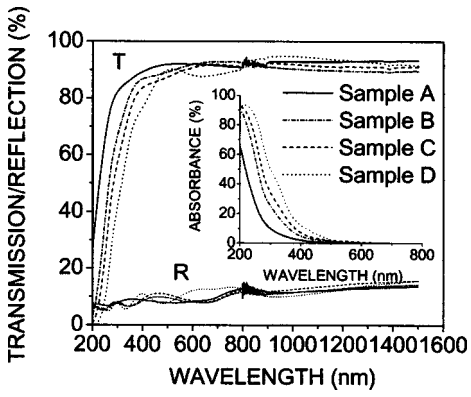

FIG. 2. Measured transmittance (T) and reflectance (R) of the A–D samples for normal (transmittance) or quasinormal (reflectance) incidence. The data are normalized with respect to air. The inset shows the absorbance (A) deduced from the measured R and T data as $A=100-R-T$. The noisy feature at about 800 nm is an experimental artifact.

TABLE II. Summary of the different waveguide parameters extracted from the *m*-line measurements, simulations, and TEM images. n_{TE} (n_{TM}) is the modal effective index for TE (TM) polarized waveguide mode, B is the modal birefringence, n_o and n_e the ordinary and extraordinary effective indices of the active superlattice, $\beta=(n_e-n_o)/n_o$ is the material effective birefringence, Γ_{TE} and Γ_{TM} the optical confinement factors for the TE and TM modes.

	B	C	D
Thickness core layer	186 nm	215 nm	295 nm
n_{TE}	1.462	1.476	1.519
n_{TM}	1.456	1.458	1.486
B	0.006	0.018	0.033
n_o	1.564	1.600	1.621
n_e	1.540	1.581	1.603
β (%)	−1.1	−1.3	−1.2
Γ_{TE} (%)	27	44	72
Γ_{TM} (%)	3	10	56

factor of the optical mode in the active superlattice layer, followed by samples C and B. In particular, the TM mode of the B sample shows very weak confinement. All the samples exhibit a very similar negative material biregringence $\beta=(n_e-n_o)/n_o$ (i.e., $n_o>n_e$), as expected in a multilayer structure. The measured value of about −1% is significantly larger than the one observed for GaAs/AlGaAs multiquantum well waveguides.[22] A more detailed report on the birefringent properties of this kind of sample has been published else where.[18]

The optical losses in the waveguide samples were measured with an experimental technique named shifting-excitation-spot (SES). SES consists of exciting the waveguide through the surface with a small laser spot of suitable wavelength and measuring the luminescence emitted from the edge as the spot position is varied along the optical mode propagation direction, *z*.[13,23–25] The luminescence intensity collected from the edge as a function of the spot position *z* is governed by Beer's law, $I(z)=I_o=I_o\exp(-\alpha z)$, where I_o is the luminescence emitted at *z* and $I(z)$ is the luminescence collected at the edge of the sample. The waveguide losses can be extracted from a fit of the SES data. Figures 3 and 4 show the SES losses obtained by excited with $a\approx 100$ μm wide Argon-ion laser spot, an excitation wavelength of $\lambda=365$ nm, and a very low laser power (few milliWatts). The trend observed in Fig. 3(b) shows that the losses decrease with increasing nanocrystal size, both for the TE and TM modes. The TM mode suffers for larger propagation losses than the TE mode because the optical confinement factor (Γ) is lower for the TM mode than for the TE (see Table II). In addition, a weak wavelength dependence of the optical losses is shown in Fig. 4 for two representative samples.

An order of magnitude of the losses in Si-nc waveguides can be calculated assuming direct absorption and Mie scattering.[26] With an absorption cross section per Si-nc of $\sigma_{abs}\sim 10^{-18}$ cm^2,[14] and a Si-nc density of $N_{Si\text{-}nc}\sim 10^{19}$ cm^{-3}, one finds a loss coefficient $\alpha=N_{Si\text{-}nc}\times\sigma_{abs}\sim 10$ cm^{-1}, which is of the same order of magnitude as that measured experiementally. This loss coefficient is also of the same order of magnitude as that calculated from Mie scattering theory.[26] Mie scattering is due to the fluctuations in the refractive index of the waveguide core caused by its composite structure (Si-nc and SiO_2). Thus, three main factors cause the losses that we have measured: electronic absorption, light diffusion due to Mie scattering, and imperfections in the waveguides (e.g., interface roughnesses). This last factor might explain the observed sample to sample variations.

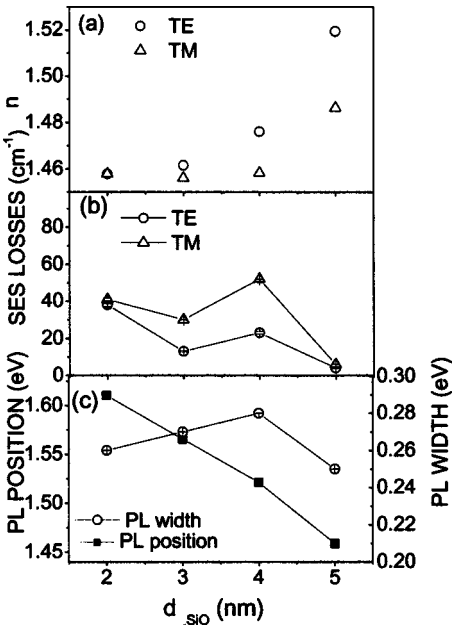

FIG. 3. (a) Transverse-electric TE (circle), and transverse-magnetic TM (triangle) effective refractive indices measured by *m*–line at 632.8 nm as a function of the nominal nanocrystals size, d_{SiO}. (b) Propagation losses as a function of d_{SiO} measured via SES technique both for TE (circle) and TM (triangle) polarized optical modes. The SES data were measured at 750 nm. (c) Spectral position of the photoluminescence maximum (square) and full width at half maximum of the photoluminescence band (circle) as a function of d_{SiO}.

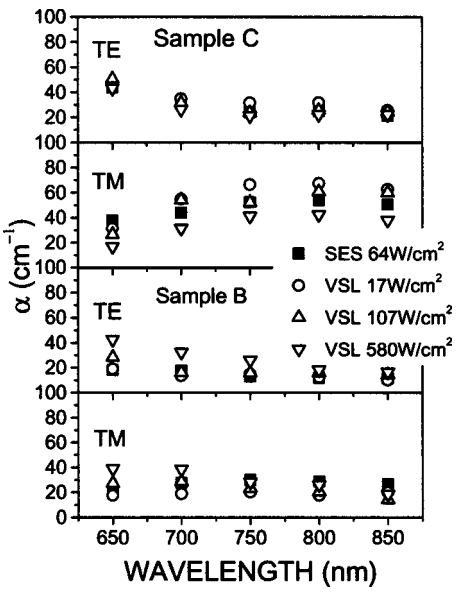

FIG. 4. Optical losses (α) of samples C and B vs wavelengths measured by SES and VSL for various pump powers and for TE or TM polarized optical modes.

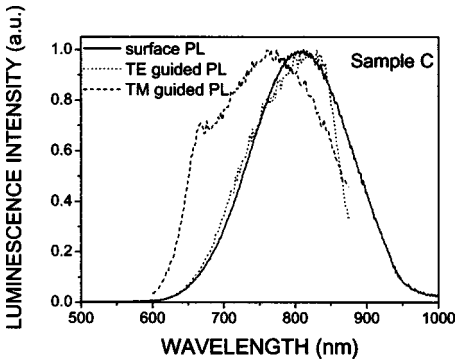

FIG. 5. Luminescence spectra measured for sample C in different geometries. Full line: luminescence collected from the sample surface. Dotted line: luminescence collected from the edge of the sample and polarized parallel to the Si-nc layers (TE polarization) when the excitation was well inside sample (large *z*). Dashed line: TM polarized luminescence. The long wavelength cutoff (880 nm) of the recording system is responsible for the long wavelength drop of the TE and TM luminescence. No similar effect is observed in surface luminescence due to a different recording system.

IV. OPTICAL PUMPING POWER MEASUREMENTS

In order to characterize the spontaneous and stimulated emission properties of the waveguides, we have performed photoluminescence and variable-stripe-length (VSL) measurements.[25]

A. Continuous-wave (cw) photoluminescence

The luminescence results are summarized in Fig. 3(c). Luminescence was collected from the surface of the sample. The maximum of the emission band [photoluminescence (PL) position in Fig. 3] blueshifts with decreasing Si-nc sizes (d_{SiO}), in accordance with a quantum-confinement based model.[27] The PL width, on the other side, is quite independent on d_{SiO}, which we attribute to the small size dispersion obtained with this growth technique.[15]

Figure 5 reports the change in the luminescence lineshape as a function of the polarization of the edge-emitted (waveguided) light when the excitation spot is well inside the sample, as in a SES experiment. Sample C is used as a representative sample. The change in the lineshape reflects the wavelength dependence of the optical losses in the waveguide. TM polarized luminescence is blue shifted with respect to the TE polarized luminescence because at long wavelengths the propagation losses for this polarization are larger than the losses for the TE polarization (Fig. 4). In fact, these spectra can be easily reproduced by making the convolution between the loss coefficients for each mode and the luminescence spectrum collected from the surface. As our waveguides are monomode, no waveguide mode filtering effects like those reported in Refs. 28 and 29 were observed.

We varied the pumping power in the high excitation regime and recorded the surface emitted luminescence. An example is reported in Figs. 6 and 7 for sample C. When the excitation wavelength is 365 nm and the pump power is increased, the luminescence intensity increases sublinearly due to Auger limited recombinations. However, its spectral position does not shift while its lineshape broadens (Fig. 6). This is in contrast with other reports, where clear and large blue

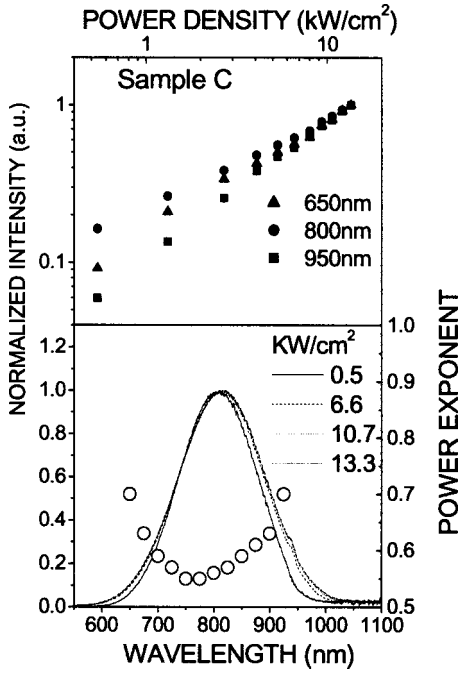

FIG. 6. (Top) Normalized intensity vs the pumping power for various wavelengths (bottom) photoluminescence spectra for different pumping powers (full line). The circles are the exponents obtained with a power law fit of the pump power dependent photoluminescence intensity. Sample C was used. The excitation wavelength was 365 nm.

shifts of the Si-nc luminescence as a function of the pumping power were observed due to the size selectivity of Auger saturation.[30] This experimental fact can be attributed to the small size dispersion in these samples, which does not allow for spectral diffusion. A power law dependence of the luminescence intensity on the pumping power is observed over a wide power range. The exponent *m* of the power laws are plotted in Fig. 6 as a function of the observation wavelength. An inverted bell shape of the power law exponent is observed in Fig. 6, which is due to the power broadening of the emission lineshape. Power broadening has been reported for transitions in two-level atomic systems and interpreted as

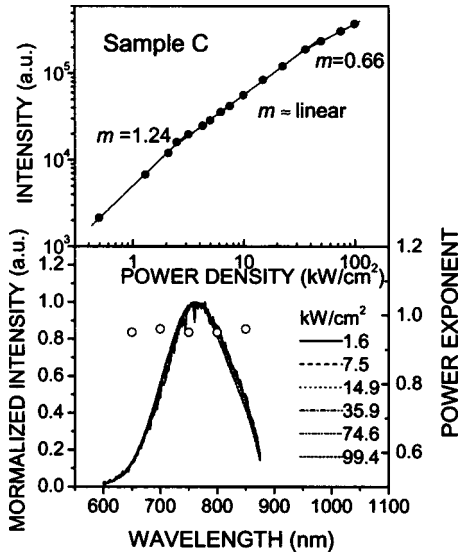

FIG. 7. Same as in Fig. 6 but with 488 nm excitation wavelength.

saturation of the optical transition.[31] If the data of Fig. 6 were interpreted in the same way, i.e., emission line saturation, it would imply an homogeneous nature of the wide emission lineshape, as has been claimed in the literature for single Si-nc experiments.[32] Homogeneous linewidth results from an ensemble of emitters when these emitters have the same emission linewidths and energies. The monodisperse nature of the Si-nc in our samples could result in an homogeneous linewidth. Similar behaviors versus pumping power are observed for other samples with typical m exponents at 750 nm of 0.7, 0.5, and 0.65 for samples A, B, and D, respectively. It is worthwhile to mention that the minimum in m is centered at a wavelength where we also observe the maximum of the amplified spontaneous emission (ASE) spectrum of the fast component in time resolved measurements (see Fig. 13).

If we perform similar experiments with a different pumping wavelength ($\lambda = 488$ nm, Fig. 7), where the absorption cross sections of the Si-nc are lower, the luminescence intensity increases linearly with the pumping power and no power broadening is observed. Only at the highest pumping powers a deviation from the linearity can be seen and the spectra start to broaden (Fig. 7). This implies that power broadening is only observed when the Auger limited recombination regime is entered.

B. Continuous-wave variable-stripe-length measurements

VSL measurements under CW excitation were performed employing the same laser source used for the SES measurements. The experimental technique has already been described in detail in several papers.[2–5] We employed all of the various experimental cares described in Ref. 25 to avoid possible experimental artefacts that had been used. The experimental data were fitted with the one-dimensional amplifier model,

$$I_{\mathrm{ASE}}(\ell) = \frac{J_{\mathrm{sp}}(\Omega)}{g_{\mathrm{mod}}}(e^{g_{\mathrm{mod}}\ell} - 1), \tag{1}$$

where I_{ASE} represents the amplified spontaneous emission intensity, ℓ is the excitation stripe length, g_{mod} is the net modal gain of the material defined as $g_{\mathrm{mod}} = \Gamma g_m - \alpha$, where Γ is the optical confinement factor of the waveguide, $J_{\mathrm{sp}}(\Omega) = (A_{\mathrm{sp}} h\nu \Omega N^*/4\pi)$ is the spontaneous emission intensity emitted within the solid angle Ω, A_{sp} is the spontaneous emission rate, N^* is the excited state population density, and $h\nu$ is the energy of the emitted photon.

Figure 4 summarizes the results for the A–D samples. For all the pump powers used, the optical gain was negative (net optical losses). For low pumping powers, optical losses comparable with the SES data were found, thus supporting the experimental confidence on the technique.[12] Increasing the pumping power up to 0.6 kW cm^2, none of the samples showed positive optical gain under CW excitation. In Ref. 33, to switch from negative to positive gain values a threshold pump power of 0.5 kW cm^2 was reported for plasma enhanced chemical vapor deposited (PECVD) Si-nc wave guides. In this work, some samples (A, B) showed losses increasing with pumping power, while sample C has losses which decrease with pumping power, and sample D show losses that are independent of pumping power. Samples E and F showed losses as large as 100 cm^{-1} due to their poor waveguiding properties.

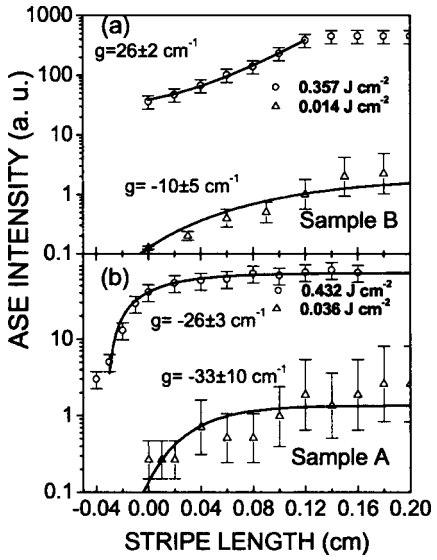

FIG. 8. (a) High (circles) and low (triangle) fluence time resolved variable stripe length TR-VSL data for sample B. The lines are fits to the data with Eq. (1). The extracted gain parameters are reported. The error bars of the optical gain values are the standard deviation of the nonlinear fits. (b) The same data for the sample A. The difference in the maximum and minimum fluence employed for the two samples is due to differences in their damage thresholds. The observation wavelength was 750 nm.

C. Pulsed variable-stripe-length measurements

We also measured the amplified spontaneous emission with the time resolved VSL measurements.[4] The laser source was the third harmonic output (355 nm) of a Nd:YAG (YAG—yttrium aluminium garnet) laser, operating at 10 Hz, with a pulse duration of 6 ns and maximum average energy of 300 m. Care was taken to maintain the laser fluence (Φ) under the damage threshold of the sample (different for each sample). No analysis in polarization of the luminescence was performed.

Optical gain is strongly dependent on the population inversion, which depends on the pumping level. If positive optical gain is observed at high Φ, it has to disappear when Φ is decreased. This control measurement has been performed for all the samples. VSL data were recorded in the first few nanoseconds after pulse excitation. Figure 8(b) shows the VSL results for sample A. Fit of the data with Eq. (1) shows that no positive optical gain is achieved in this sample even under high Φ. On the contrary, sample B [Fig. 8(a)] shows a positive optical gain $g = 26 \pm 2$ cm^{-1} at $\Phi = 357$ mJ/cm^{-2} while losses are observed at $\Phi = 14$ mJ/cm^{-2}. Samples B and C did show positive optical gain under high fluence conditions, while samples E, F, A, and D did not (Fig. 9).

Furthermore, we observed that when pumped with high Φ, the sample emission develops a fast nanosecond decay superimposed on the usual microsecond emission decay.[4,5]

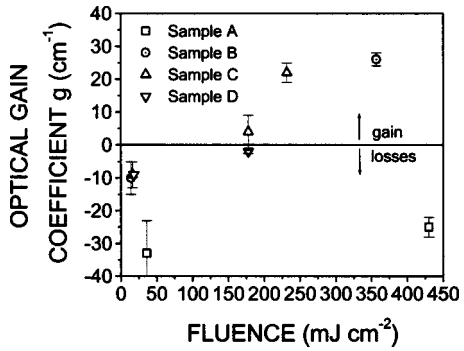

FIG. 9. Summary of gain values obtained from the fit of the TR-VSL curves with Eq. (2) vs the excitation fluence. The different symbols (explained in the figure's legend) refer to the various samples. The error bars of the optical gain values are the standard deviation of the nonlinear fits. The observation wavelength was 750 nm.

We looked at the Φ and ℓ dependence of this fast decay component. Figure 10 shows the I_{ASE} time decay for samples A and B. When the sample is showing positive optical gain in VSL, as for sample B, the fast (nanoseconds) component disappears for both decreasing Φ and ℓ, as found in Refs. 4 and 5. On the contrary, when the sample shows optical losses in VSL, as for sample A, the fast component disappears at low Φ but is observed at high Φ for long as well as short ℓ. This difference is very important. In Ref. 4, we proposed a model for the fast component of the decay in the VSL configuration that takes into account both stimulated emission and Auger nonradiative recombination effects. It was argued that the time decay dynamics of I_{ASE} is governed by the interplay between these two effects. From a rate equation analysis, a stimulated emission lifetime τ_{se} can be defined as[4]

$$\tau_{\mathrm{se}} = \frac{\frac{4}{3}\pi {R_{\mathrm{nc}}}^3}{\xi \sigma c n_{\mathrm{ph}}}, \tag{2}$$

where R_{nc} is the average Si-nc radius, ξ is the Si-nc volume fraction, σ is the emission cross section per nanocrystal, and n_{ph} is the number of emitted photons. An effective Auger recombination time can also be defined as

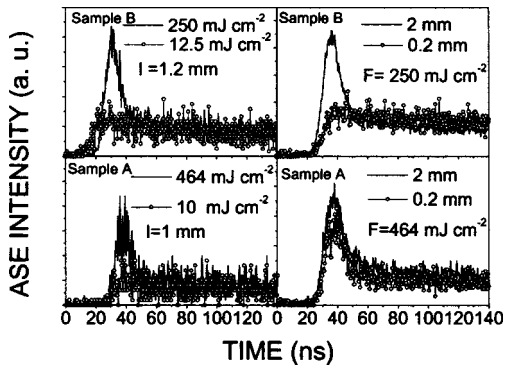

FIG. 10. Top left panel: power dependence of TR-VSL decay for a fixed stripe length of 1.2 mm (sample B). Top right panel: stripe length dependence of TR-VSL decay for a fixed pump fluence of 250 mJ/cm^{-2} (sample B). Bottom left panel: power dependence of TR-VSL decay for a fixed stripe length of 1 mm (sample A). Bottom right panel: stripe length dependence of TR-VSL decay for a fixed pump fluence of 464 mJ/cm^{-2} (sample A).

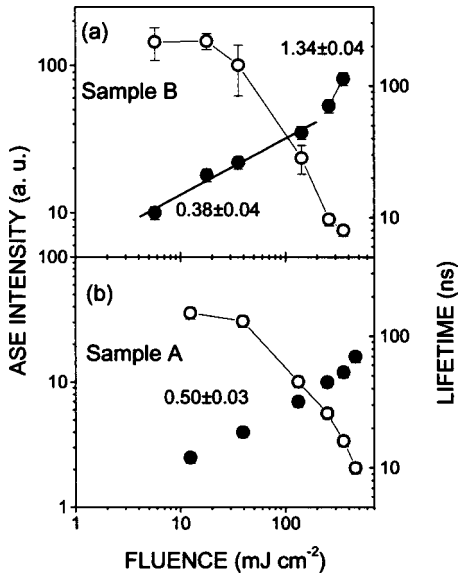

FIG. 11. Fluence dependence of ASE intensity (peak intensity of fast component in the TR-VSL decay, disks) and of the fast component lifetime (calculated as the $1/e$ value, empty circles) for sample B (a) and sample A (b). The reported numbers are the results of power law fits (lines) to the ASE intensity. The observation wavelength was 750 nm and the excitation stripe length was, respectively, 0.1 cm for sample A and 0.12 cm for sample B.

$$\tau_A = \frac{1}{2C_A N}, \tag{3}$$

where C_A is an effective Auger coefficient and N is the density of photoexcited electron-hole pairs. Hence, when the fast decay is dominated by stimulated emission, it will depend on the photon density, i.e., on I_{ASE}: as ℓ decreases, the photon density decreases too, and the fast component disappears (sample B, Fig. 10). When the fast decay is dominated by Auger recombination, it will depend on the density of photoexcited electron-hole pairs, i.e., on Φ: a decrease of ℓ does not affect Φ, which, in turn means the same N, and the fast component is still observed (sample A, Fig. 10). Additionally, decreasing Φ while keeping fixed ℓ (Fig. 10, left panels), the fast component disappears for both the samples. When Auger is dominating, this is due to the decrease of N, while, dominant stimulated emission corresponds to a decrease of the inversion factor (i.e., gain) in the sample. In both cases, some additional processes might contribute to further shortening of the lifetime with increasing Φ, like carrier migration and thermalization in silicon nanocrystals.[34]

The I_{ASE} peak intensities and I_{ASE} fast lifetimes for long ℓ are plotted as a function of the incident Φ in Fig. 11. A smooth threshold behavior from a saturation to a superlinear increase is observed for sample B, while no threshold is observed for sample A. For sample B under the threshold, the intensity increases with a typical Auger limited behavior.[35,36] When the threshold is exceeded, the intensity increase is more than linear and the fast-component lifetime shortens significantly. Due to sample damage at higher Φ, the number of data points is limited for high Φ. Sample A, on the other hand, shows a sublinear increase of the luminescence inten-

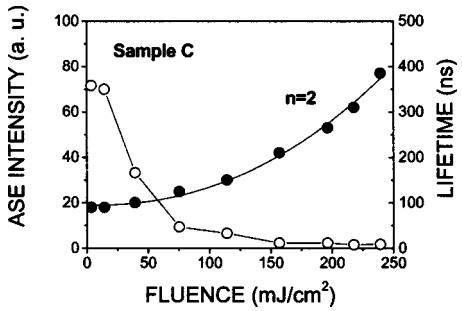

FIG. 12. Fluence dependence of ASE intensity (peak intensity of the fast component in the TR-VSL decay, disks) and of the fast component lifetime (calculated as the $1/e$ value, empty circles) for sample C. The exponent n of the power law fit of the ASE intensity is reported. The wavelength was 750 nm.

sity for all Φ. The fast component lifetime of sample A is seen to decrease according to the excited electron-hole pair density dependence of the Auger lifetime.

For clarity we have presented experimental data only for samples A and B. However, similar data have been measured for all the samples. Samples E, F, and D show behaviors similar to that observed for sample A, while sample C shows optical gain at high fluence and a behavior similar to sample B (Fig. 12).

Time resolved spectra at high Φ for the different samples are shown in Fig. 13. The fast component I_{ASE} spectrum is centered at about 780 nm for samples B and C, even if the microsecond integrated emission spectra (lines in Fig. 13) are centered at different wavelengths (which are very close to the low power CW surface emitted luminescence spectra, see Fig. 3). Sample A shows a fast component spectrum centered at about 725 nm, while the slow component spectrum is slightly redshifted to 730 nm. The similarity in the fast component I_{ASE} spectra of samples B and C suggests that the

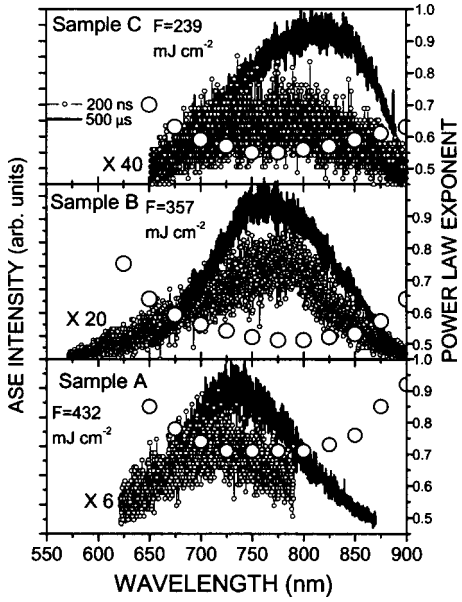

FIG. 13. High fluence (F) TR-VSL luminescence spectra integrated over short (200 ns, circles) and long (500 μs, lines) temporal windows for samples A, B and C. The intensity scale is arbitrary. Big circles refer to the power law exponent extracted from the CW luminescence intensity dependence on the pump power (Fig. 6).

levels responsible for the population inversion, i.e., for the optical gain, have the same nature in samples B and C. A model was proposed in Ref. 4, where emission under CW excitation and in the microsecond integrated luminescence is due to excitonic recombinations in quantum confined nanostructures, while stimulated emission is due to the recombination involving the interface states between a stressed SiO_2 and the Si-nc.[13]

The spectra are superimposed on the power law exponents of the integrated intensity dependence on the pumping power and measured under CW excitation at different wavelengths. It is clear that the inverted bell shape of the exponent curves is concomitant, in the samples showing positive net optical gain (samples B and C), to the fast component time resolved spectrum maximum.

V. DISCUSSION

Figure 9 shows a summary of the experimental data about the gain coefficient for samples A–D, i.e., the samples that behave as a waveguide. It is clear from the figure that the key parameters allowing observation of positive optical gain are high optical damage threshold combined with a good waveguide structure containing properly sized silicon nanocrystals. Sample D can be photoexcited up to nearly the transparency regime (i.e., $g \approx 0$) before sample damage occurs. Sample A has the largest losses and poorest optical confinement in the active layer. No net optical gain is observed in this sample.

In these samples we were able to observe gain only under pulsed excitation, while, in PECVD grown Si-nc waveguides, gain was observed also under CW conditions.[33] In Ref. 10, a similar phenomenology was reported: no gain under CW excitation and gain under pulsed excitation. There, it was claimed that a negative role was played by thermal heating of the sample, which is largest under CW pumping; a similar explanation can be applied also here.

By comparing the data of Fig. 9 with those of Table II, no correlation emerges between the presence of high material birefringence and the presence of optical gain, but it is clear that a birefringent structure is not detrimental for the observation of optical gain. It can be expected anyhow from what is observed in Sec. IV, namely, that the stimulated emission propagates preferentially along the more efficiently confined TE mode. Polarization resolved VSL measurements would be needed to confirm this point and are planned for the near future.

Only samples B and C show positive optical gain. The gain values are higher than those previously reported for samples grown by PECVD (Ref. 4) and lower than those reported for samples grown by magnetron sputtering.[10] We must note that the optical confinement for the waveguide of Ref. 10 was almost 100%, while here lower values have been estimated (Table II). Hence these samples show larger material gain values than in Refs. 4 and 10, which could be due to the small size dispersion typical of Si-nc in these samples.

Figure 13 shows that the saturation of the luminescence is stronger where stimulated emission is larger (best seen in sample C). Indeed, the power law exponents of the sublinear

dependence of the luminescence have a minimum where the fast component of I_{ASE} due to stimulated emission has a maximum. At the moment we lack a clear theory of this power broadening phenomenon, and the correspondence shown in Fig. 13 is simply a hint towards an explanation that could couple the power broadening to the observed optical gain.

VI. CONCLUSIONS

In conclusion, we have demonstrated the presence of positive optical gain under pulsed excitation, in silicon monodispersed-nanocrystals waveguides grown via evaporation and crystallization driven by high temperature annealing. The small size dispersion of Si-nc could explain the large material gain and the presence of power broadening of the luminescence. The optical gain is found to be correlated with a good waveguide structure (low losses and large optical mode confinement), high damage threshold under UV light irradiation, and the monodispersive nature of properly sized silicon nanocrystals. One issue that emerges from this study is the problem of thermal management in Si-nc waveguides to maximize gain and reduce the optical damage of the waveguide.

ACKNOWLEDGMENTS

This work has been supported by the INFM advanced research project RAMSES, by CE through the SINERGIA project, and by the DFG (Za191/13-1). The valuable collaboration of Dr. L. Dal Negro (now at MIT, Boston, USA) on the physics of gain in Si-nc and the reading of Dr. W. J. Weber is gratefully acknowledged.

[1]D. A. B. Miller, Proc. IEEE **88**, 728 (2000); *Silicon Photonics*, edited by L. Pavesi and D. Lockwood (Springer, Berlin, 2004).
[2]L. Pavesi, J. Phys.: Condens. Matter **15**, R1169 (2003); *Towards the First Silicon Laser*, edited by L. Pavesi, S. Gaponenko, and L. Dal Negro (Kluwer, Dordrecht, 2003).
[3]L. Pavesi, L. Dal Negro, C. Mazzoleni, G. Franzò, and F. Priolo, Nature (London) **408**, 440 (2000).
[4]L. Dal Negro, M. Cazzanelli, L. Pavesi, S. Ossicini, D. Pacifici, G. Franzò, F. Priolo, and F. Iacona, Appl. Phys. Lett. **82**, 4636 (2003).
[5]L. Khriachtchev, M. Rasanen, S. Novikov, and J. Sinkkonen, Appl. Phys. Lett. **79**, 1249 (2001).
[6]M. Nayfeh, S. Rao, N. Barry, A. Smith, and S. Chaieb, Appl. Phys. Lett. **80**, 121 (2002).
[7]K. Luterova, I. Pelant, I. Mikulskas, R. Tomasiunas, D. Muller, J. J. Grob, J. L. Rehspringer, and B. Hönerlage, J. Appl. Phys. **91**, 2896 (2002).
[8]H.-S. Han, S.-Y. Seo, and J. H. Shin, Appl. Phys. Lett. **79**, 4568 (2001).
[9]H.-S. Han, S.-Y. Seo, J. H. Shin, and N. Park, Appl. Phys. Lett. **81**, 3720 (2002).
[10]J. Ruan, P. M. Fauchet, L. Dal Negro, M. Cazzanelli, and L. Pavesi, Appl. Phys. Lett. **83**, 5479 (2003).
[11]R. G. Elliman, M. J. Lederer, N. Smith, and B. Luther-Davies, Nucl. Instrum. Methods Phys. Res. B **206**, 427 (2003).
[12]J. Valenta, I. Pelant, and J. Linnros, Appl. Phys. Lett. **81**, 1396 (2002).
[13]N. Daldosso *et al.*, Phys. Rev. B **68**, 085327 (2003).
[14]L. Khriachtchev *et al.*, Appl. Phys. Lett. **81**, 1357 (2002).
[15]M. Zacharias, J. Heitmann, R. Scholz, U. Kahler, M. Schmidt, and J. Bläsing, Appl. Phys. Lett. **80**, 661 (2002); M. Zacharias, L. X. Yi, J. Heitmann, R. Scholz, M. Reiche, and U. Gösele, Solid State Phenom. **54**, 95 (2003).
[16]L. X. Yi, J. Heitmann, R. Scholz, and M. Zacharias, Appl. Phys. Lett. **81**, 4248 (2002).
[17]P. D. Townsend, G. L. Baker, N. E. Schlotter, C. F. Klausner, and S. Etemad, Appl. Phys. Lett. **53**, 1782 (1988); P. K. Tien, R. Ulrich, and R. J. Martin, *ibid.* **14**, 291 (1969).
[18]F. Riboli *et al.*, Appl. Phys. Lett. **85**, 1268 (2004).
[19]C. J. Oton, Z. Gaburro, M. Ghulinyan, L. Pancheri, P. Bettotti, L. Dal Negro, and L. Pavesi, Appl. Phys. Lett. **81**, 4919 (2002).
[20]A. Yariv and P. Yeh, *Optical Waves in Crystals* (Wiley-Interscience, New York, 1984).
[21]W. Theiss, Surf. Sci. Rep. **29**, 91 (1997).
[22]J. Kang *et al.*, IEEE Photonics Technol. Lett. **7**, 769 (1995).
[23]P. C. Mogensen, P. M. Smowton, and P. Blood, Appl. Phys. Lett. **71**, 1975 (1997).
[24]P. M. Smowton, E. Herrmann, Y. Ning, H. D. Summers, P. Blood, and M. Hopkinson, Appl. Phys. Lett. **78**, 2629 (2001).
[25]L. Dal Negro, P. Bettotti, M. Cazzanelli, L. Pavesi, and D. Pacifici, Opt. Lett. **229**, 337 (2004).
[26]H. C. van de Hulst, *Light Scattering by Small Particles* (Dover, New York, 1981).
[27]V. Lehmann and U. Gösele, Appl. Phys. Lett. **58**, 856 (1991).
[28]L. Khriachtchev, M. Räsänen, and S. Novikov, Appl. Phys. Lett. **83**, 3018 (2003).
[29]J. Valenta, I. Pelant, K. Luerová, R. Tomasiunas, S. Cheylan, R. G. Elliman, J. Linnros, and B. Hönerlage, Appl. Phys. Lett. **82**, 955 (2003).
[30]D. Amans, O. Guillois, G. Ledoux, D. Porterat, and C. Reynaud, J. Appl. Phys. **91**, 5334 (2002).
[31]M. L. Citron, H. R. Gray, C. W. Gabel, and C. R. Stroud, Jr., Phys. Rev. A **16**, 1507 (1977).
[32]J. Valenta, R. Juhasz, and J. Linnros, Appl. Phys. Lett. **80**, 1070 (2002).
[33]L. Dal Negro *et al.*, Physica E (Amsterdam) **16**, 297 (2003).
[34]L. Pavesi, J. Appl. Phys. **80**, 216 (1996).
[35]L. Dal Negro, PhD thesis, Università di Trento, 2003.
[36]R. M'ghaieth, H. Maaref, I. Mihalcescu, and J. C. Vial, Phys. Rev. B **60**, 4450 (1999).